GEOCHEMISTRY

Paleozoic carbonatites controlled rare-earth-elements mineralization at Bayan Obo

Yang Li[1,2,3]*, Li-Guang Wu[4], Yan Yu[4], Lan Yang[4], David Selby[5], Xian-Hua Li[4]*

The net-zero emission race drives the consumption of rare-earth-elements (REE) at an accelerated rate. With the demand of REE being met by a few giant deposits such as Bayan Obo, decoding controls of ore formation is vital. Yet, after nearly a century of study, the genesis of Bayan Obo remains debated. Here, we demonstrate that two stages of carbonatites emplaced at Bayan Obo at 1320 and 430 million years ago (Ma). The effusive nature of the 1320 Ma carbonatite suppressed brine/fluid exsolution; hence, mineralization at this stage is limited, but its subsequent deformation created an ideal environment for water-rock interaction induced mineralization. The 430 Ma carbonatites exsolved voluminous brine/alkaline fluids rich in REE, with mineralization being promoted as veins and along beddings of the deformed Mesoproterozoic carbonatites via metasomatism. This stage contributed >70% REE. Our study highlights that multistage carbonatites emplaced at one locality could be a controlling factor for REE mineralization and explains the scarcity of giant deposits.

INTRODUCTION

Driven by climate change mitigation, the demand of rare-earth-elements (REE), a group of elements widely used to build low-carbon energy devices and infrastructure, increases rapidly (*1*). Increasing demand of REE and the scarcity of giant REE deposits highlight the importance of understanding how world-class deposits form—a prerequisite for successful exploration and efficient mining. Unlike their name suggests, REE are not rare in Earth's crust and are preferentially enriched in carbonatites (*2*). Of the 676 carbonatites found globally, at least 61 contain established mineral reserves (Fig. 1A). With 9% known carbonatites being mineralized, REE is one of the easiest metals to form a deposit (Fig. 1B), which is in sharp contrast to the typical barren nature of granites for Cu and Au. However, the total number of carbonatites found so far is rather limited ($n = 676$; Fig. 1A); hence, ore-bearing carbonatites are rare ($n = 61$) and exhibit an uneven global distribution (Fig. 1A). Consequently, the world's REE reserve and supply are dominated by a few giant deposits (Fig. 1A). In 2023, Bayan Obo (China) and Mountain Pass (Unites States) supplied more than 60% and more than 10% of the global production of light-REE (LREE), respectively (*3*).

The challenges in establishing a coherent genetic model for giant REE deposits are best illustrated by Bayan Obo (Fig. 2), which contains 100 million metric tons (Mt) of REE_2O_3 reserve with an average grade of 5.6% and has supplied 57% of the historical REE to the global market (*3*,*4*). At Bayan Obo, mineralization is mostly hosted by a stratiform unit known as H8 dolomite (termed as H8 unit hereafter), which extends for 16 km with a width of 2 to 4 km (Fig. 2, A to C). A characteristic feature of REE ores hosted by the H8 unit is their banding textures with a thickness of a few millimeters to tens of centimeters, which were crosscut by vein-type mineralization (fig. S1). The banded ores generally show textures of deformation and foliation (i.e., folding and fish microstructures; fig. S1A), but the presence of banded ores without deformation (fig. S1B) raises the possibility that they may have inherited the deformed pseudomorph of primary rocks through metasomatism. Mineralization as veins crosscutting banded ores is undeformed (fig. S1B).

Debates on the genesis of Bayan Obo are mainly focused on the origin of ore-hosting H8 unit (either sedimentary carbonate or igneous carbonatite), timing of mineralization, and the source of ore-forming fluids (Fig. 2D). The stratiform morphology and the banded textures of the H8 unit (fig. S1) are used to argue for a Mesoproterozoic sedimentary origin, with REE mineralization being attributed to a Paleozoic-aged metasomatism event (*4*). In this sedimentary-metasomatism model, ore-forming fluids were sourced from subduction plate dehydration, with REE being extracted from hypothetical carbonatites sitting in the upper mantle (*5*), middle crust (*6*), or lower crust (*7*). In contrast, a 1320 Ma ^{147}Sm-^{143}Nd errorchron for a carbonatite dike at the east contact zone (known as the Wu dike, Fig. 2 and fig. S2D) and the elemental and isotopic similarity between the Wu dike and portions of the H8 unit are used to suggest a Mesoproterozoic carbonatitic origin for the H8 unit (*8*–*10*). In this carbonatitic model, REE mineralization was directly linked to the Mesoproterozoic carbonatite (*11*–*13*) but was remobilized over a billion-year-long interval by metamorphic fluids derived from nearby sedimentary rocks (*14*). In addition, a few studies argue for a Paleozoic source of REE from subduction-derived fluids (*5*–*7*). The potential presence of multistage carbonatites has been proposed (*15*, *16*) yet lacks convincing geological and chronological evidence. To test these competing hypotheses, accurate timing of carbonatites and mineralization under a robust geological framework are fundamental, which is the major rationale of this study.

RESULTS

Carbonatite zircon U-Pb petrochronology

We mapped the distribution of carbonatite dikes across Bayan Obo, and in total, more than 60 dikes were identified (Fig. 2B). For 22

[1]Ministry of Education Key Laboratory of Orogenic Belts and Crustal Evolution, School of Earth and Space Sciences, Peking University, Beijing 100871, China. [2]Xinjiang Institute of Ecology and Geography, Chinese Academy of Sciences, Urumqi, Xinjiang 830011, China. [3]London Geochronology Centre, Department of Earth Sciences, University College London, London WC1E 6BT, UK. [4]State Key Laboratory of Lithospheric and Environmental Coevolution, Institute of Geology and Geophysics, Chinese Academy of Sciences, Beijing 100029, China. [5]Department of Earth Sciences, Durham University, Durham DH13LE, UK.
*Corresponding author. Email: geoliy@outlook.com (Y.L.); lixh@gig.ac.cn (X.-H.L.).

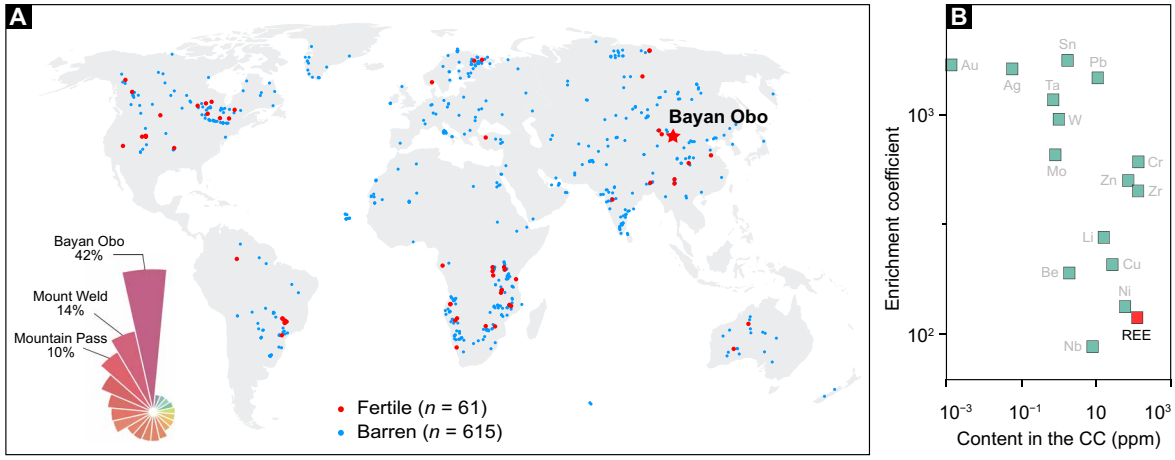

Fig. 1. Global distribution of carbonatite-related REE deposits and enrichment coefficient of REE and other metals. (**A**) Global distribution of mineralized and barren carbonatites. The insert highlights the dominant contribution of Bayan Obo to the global REE reserve. Data are compiled in data S8 and S9 (*67*–*70*). (**B**) Enrichment coefficient of metals in the continental crust (CC). The enrichment coefficient of REE is calculated relative to carbonatites, which is at the low end among other metals (in relative to CC); hence, REE are not rare in carbonatites, as supported by the observation that at least 9% of known carbonatites are mineralized. ppm, parts per million.

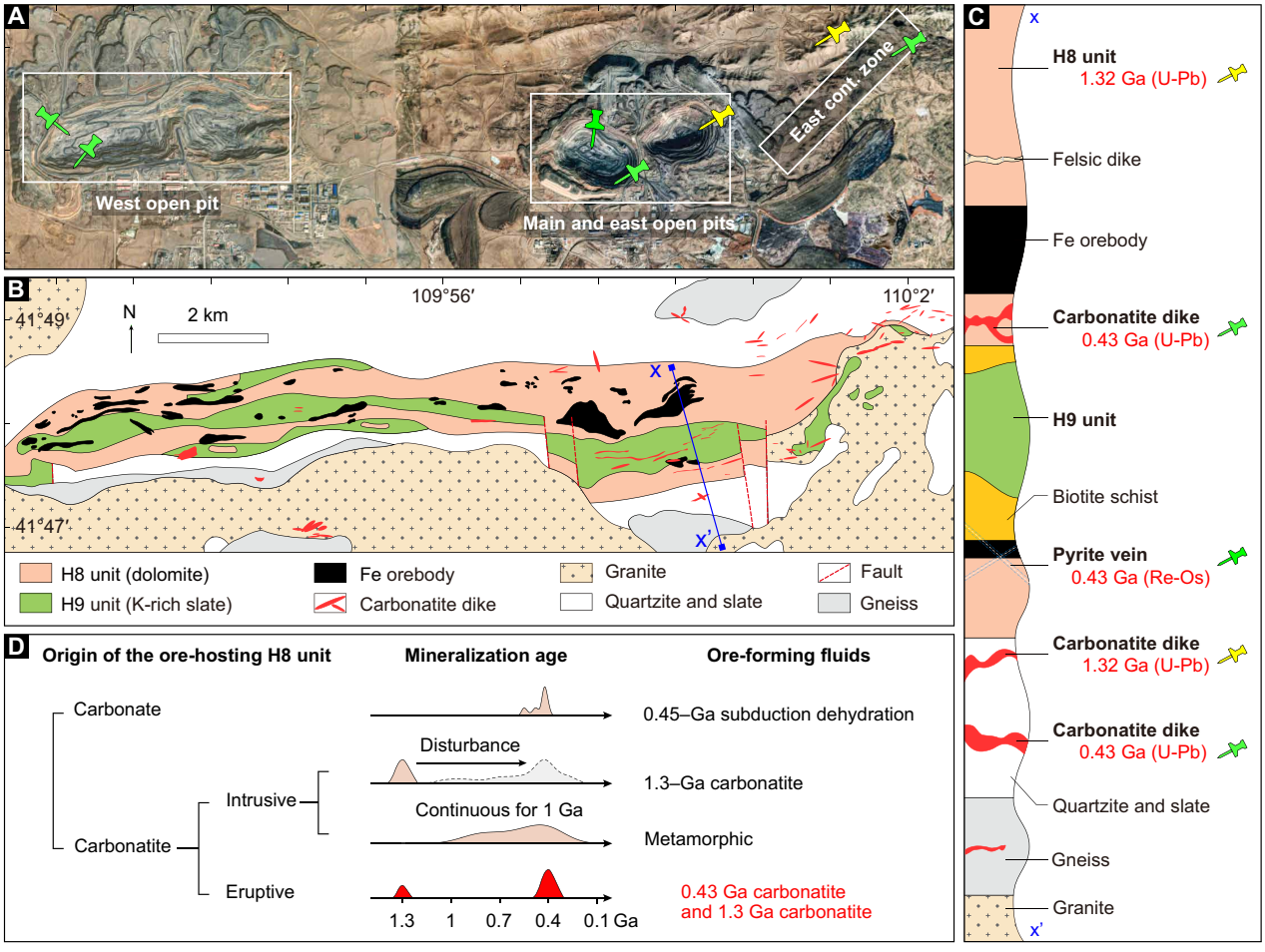

Fig. 2. Geological map of the Bayan Obo deposit and genetic debates. (**A**) Satellite image showing the distribution of west, main, and east open pits as well as the east contact zone. Sample locations are shown by a pin symbol. (**B**) Geological map. (**C**) Representative cross section (X-X′). Revised from Li *et al.* (*54*). Also shown in (C) are radiometric ages obtained in this study. (**D**) A comparison of four genetic models proposed for the Bayan Obo deposit based on origin of the ore-hosting H8 unit, timing of mineralization, and nature/source of ore-forming fluids. The main breakthrough of this study is identifying the controlling factor of the ca. 430 Ma carbonatites on REE mineralization.

dikes we have analyzed, 10 are calcium-rich (Ca-rich) carbonatite, 10 are magnesium-rich (Mg-rich) carbonatite, and the remaining 2 are intermedia (fig. S3).

Zircons were isolated from seven outcrops both within and outside the mining area (Fig. 2A). These include two carbonatite outcrops in the west open pit, a carbonatite dike in the main open pit, a carbonatite outcrop in the east open pit, two carbonatite dikes at the east contact zone, and the Wu dike at the east contact zone. We successfully obtained zircon U-Pb dates (Fig. 3 and figs. S4 to S9) for the seven carbonatite outcrops using secondary ion mass spectrometry (SIMS).

The ore-hosting H8 unit (41°48′5.1″N, 109°59′9.1″E) sampled in the east open pit is extensively altered (fig. S4). Its zircons ($n = 23$) are characterized by a triangle shape with weak zonation (100 to 200 μm in size, Fig. 3A). These zircons are relatively fresh except for a few grains that are associated with biotite and riebeckite assemblages (fig. S4). The U-Pb systematics yield a concordia date at 1321 ± 9 Ma [ca. 6 parts per million (ppm) of U; Fig. 3A].

The sandstone-hosted Wu dike (41°48′58.3″N, 110°0′49.8″E) at the east contact zone (fig. S5) is Ca-rich with strong Fe and REE mineralization at its margins (*8*, *10*). Zircons from the Wu dike are extensively altered across the entire crystals, but their overall morphology is retained (Fig. 3B). Their U-Pb dates ($n = 23$) exhibit the feature of Pb loss with an imprecise upper-intercept date of 1320 ± 110 Ma. The best-preserved zircons ($n = 9$) yield a U–Pb concordia date of 1293 ± 26 Ma (ca. 14 ppm U; Fig. 3B).

An ore-hosting carbonatite sample (41°47′48.3″N, 109°51′20″E) from a pit wall in the west open pit is Ca-rich and coarse-grained

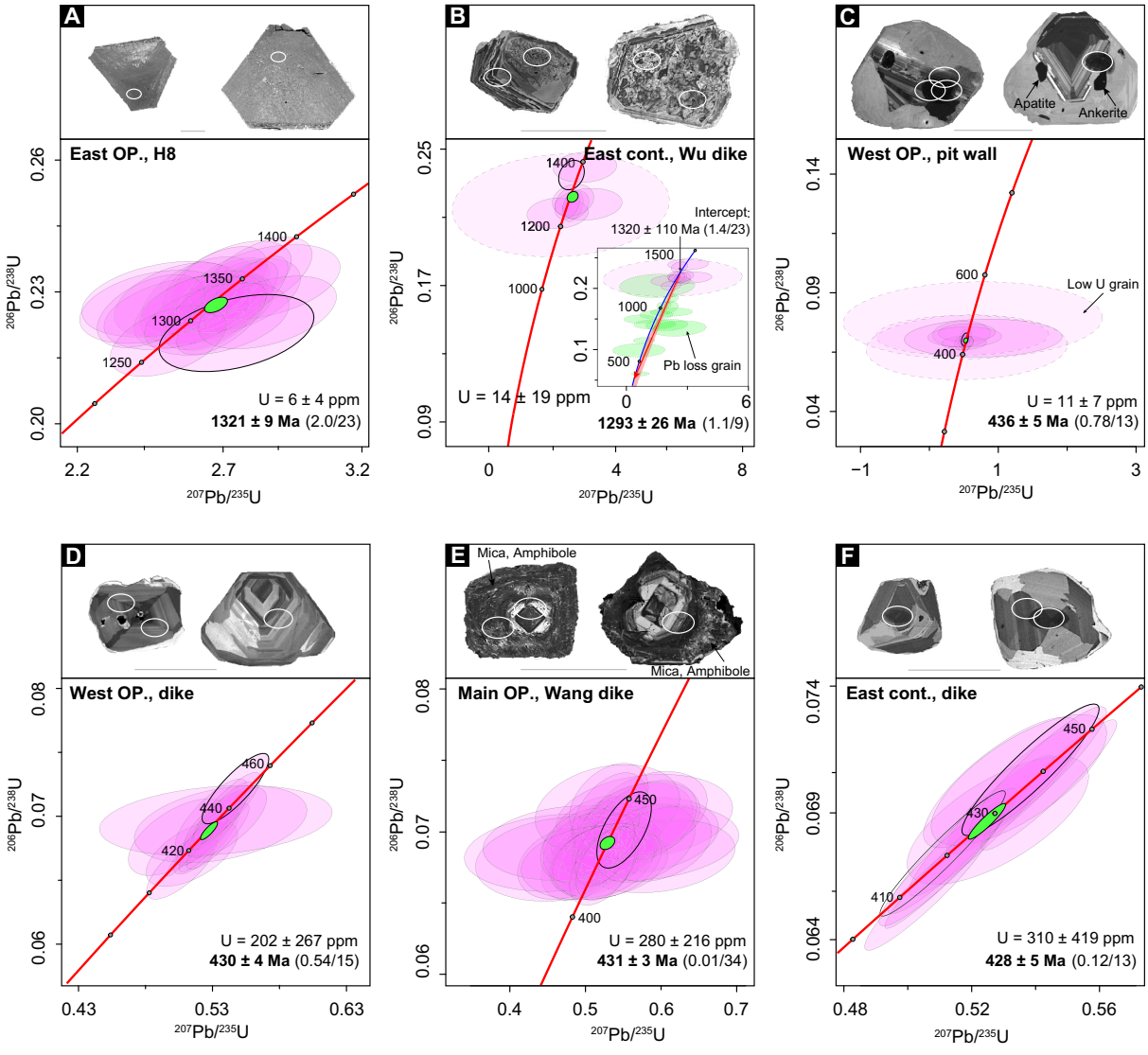

Fig. 3. Zircon U-Pb geochronology of carbonatites at Bayan Obo. Representative zircon grains and Wetherill concordia diagrams for carbonatites. (**A**) H8 unit in the east open pit (OP.). (**B**) Wu dike from the east contact (cont.) zone; the insert highlights zircon grains with Pb loss. (**C**) Pit wall carbonatite from the west open pit. (**D**) Carbonatite dike from the west open pit. (**E**) Carbonatite dike from the main open pit. This dike is named Wang dike after K.-Y. Wang. (**F**) Carbonatite dike hosted by sandstone at the east contact zone. Scale bars, 50 μm (for zircon grains). Analytical position of ion probe is shown as 10- to 15-μm ellipses. Average U contents and concordia U-Pb dates are given at the 2σ confidence level. Mean squared weighted deviation (MSWD), and number of analyses (N) are given as MSWD/N in brackets.

(fig. S6). Zircons from this sample have a partially preserved core with oscillatory zonation and an overgrowth rim without zoning (Fig. 3C). The U-Pb systematics of the cores ($n = 13$) yield a concordia age at 436 ± 5 Ma (ca. 11 ppm of U; Fig. 3C). The zircon rims were not dated due to low U contents (<0.01 ppm).

A Mg-rich carbonatite dike (41°48′2″N, 109°50′44.4″E) emplaced into the H8 unit in the west open pit is coarse-grained and moderately altered (fig. S7). Zircons from this dike are unaltered and have patched and oscillatory zoning (Fig. 3D). The U-Pb systematics ($n = 15$) yield a concordia date at 430 ± 4 Ma (ca. 202 ppm of U; Fig. 3D).

A carbonatite dike (41°47′39.5″N, 109°58′19.5″E) hosted by the H8 unit and H9 slate in the main open pit is Mg-rich, coarse-grained, and experienced extensively alteration with strong REE mineralization (fig. S8). We name this dike as Wang dike after K.-Y. Wang (*17*, *18*). Zircons from the Wang dike have a rhombus core with oscillatory zoning and a sub-rounded rim with weak zoning, and occasionally presence of mineral inclusions that include amphibole, mica, and monazite (Fig. 3E). The U-Pb systematics ($n = 34$) yield a concordia date at 431 ± 3 Ma (ca. 280 ppm of U; Fig. 3E).

Two Ca-rich, coarse-grained carbonatite dikes (41°48′47.8″N, 110°1′39.8″E and 41°48′51″N, 110°1′43″E) at the east contact zone hosted by sandstones bear disseminated Fe and REE mineralization (fig. S9). Zircons ($n = 13$) from these two dikes have patched and oscillatory zoning and yield a U-Pb concordia date at 428 ± 5 Ma (ca. 310 ppm of U; Fig. 3F).

Bastnäsite and monazite ^{232}Th-^{208}Pb and trace elements for concentrated ore samples

Our major rationale here is to yield a representative sample set to statistically assess the proportional contribution of mineralization from each ore-forming stage (i.e., how many grains are ~1320 or ~430 Ma). Considering the highly heterogeneous ^{232}Th-^{208}Pb dates observed at hand specimen scale, samples from limited outcrops likely will give different age spectrums, i.e., ^{232}Th-^{208}Pb dates from the Wu dike and Wang dike will cluster at 1320 and 430 Ma, respectively. Here, we propose that using concentrated ore samples from long-term mining, in an analogous to detrital mineral provenance studies (Fig. 4A), is an excellent approach to quantify the contribution of metal endowment through time. Four concentrated ore samples spanning a ~12-year mining history (2009, 2012, 2016, and 2020; fig. S10) were dated using ^{232}Th-^{208}Pb of bastnäsite and monazite. Bastnäsite and monazite are the two principal REE ore minerals at Bayan Obo. They are uranium-poor (U-poor; mode < 0.1 ppm) with mode Th contents of 300 and 1300 ppm, respectively (fig. S11 and data S3 and S4). They also contain high common Pb (defined as f_{208}%) with a mean of 22% for bastnäsite and 15% for monazite.

Without common Pb correction, the ^{232}Th-^{208}Pb dates are biased to much older values by an average of 75% for bastnäsite and 40% for monazite (Fig. 4, B and C), highlighting the importance of common Pb correction in ^{232}Th-^{208}Pb dating at Bayan Obo. The U-poor nature of our samples permits using ^{207}Pb instead of ^{204}Pb as a proxy for common Pb correction for improved accuracy and precision. To account for the highly variable isotope composition of common Pb at Bayan Obo, we used measured ^{208}Pb/^{207}Pb of galena (2.42 ± 0.02, $n = 10$; fig. S13) closely associated with REE mineralization instead of following the terrestrial Pb isotope evolution model. After common Pb correction, bastnäsite ^{232}Th-^{208}Pb dates vary between 244 ± 18 and 1008 ± 40 Ma ($n = 879$; Fig. 4D), with a major peak at 426 Ma (56%) and two smaller peaks at ~630 Ma (16%) and ~780 Ma (11%; table S1). Similarly, monazite ^{232}Th-^{208}Pb dates vary between 223 ± 24 and 1223 ± 112 Ma ($n = 475$; Fig. 4E), with a major peak at 429 Ma (56%) and a smaller peak at ~710 Ma (20%; table S1). For both minerals, ^{232}Th-^{208}Pb dates at 1320 Ma are negligible (<1%) and at 270 Ma are <5% (Fig. 4, D and E, and table S1).

The Ce/Y elemental ratio is significantly higher at ca. 430 Ma: Ce/Y ratio evolving from 300 to 800 to 400 to 1700 for bastnäsite ($n = 879$; Fig. 4D and fig. S14), and from 100 to 300 to 100 to 700 for monazite ($n = 475$; Fig. 4E and fig. S14). Similar data processing of published data reveals an identical increase in the Ce/Y ratio at ca. 430 Ma (fig. S15).

Pyrite Re-Os isochron geochronology

Pyrite was obtained from a banded ore sample located at the bottom of the main open pit (41°47′51.19″N, 109°58′4.52″E). Banded ores consist mainly of bastnäsite, monazite, fluorite, apatite, barite, dolomite, aegirine, and riebeckite (fig. S16A). The pyrite veins both cut across the banded ore and grow along the bedding layers (fig. S16, A and B). Some pyrites are anhedral to subhedral and are closely associated with pyrrhotite, magnetite and REE minerals (fig. S16, B and D). Other pyrite is >2-mm subhedral to euhedral cube aggregates and closely intergrown with magnetite (fig. S16C). Pyrite separates from the REE-bearing banded ore yield an isochron age of 431 ± 3 Ma ($n = 5$, mean square weighted deviation = 0.1; initial ^{187}Os/^{188}Os = 0.52 ± 0.09; fig. S17).

DISCUSSION

The geochronological challenges at Bayan Obo

Constraining the age of carbonatites and mineralization at Bayan Obo is extremely difficult due to (i) the scarcity of minerals that can be dated with sufficient precision and accuracy and (ii) data interpretation without ambiguity. Here, we first discuss the strength and weakness of relevant isotopic systems and then compile and analyze existing data before exploring avenues for improved geochronology.

The ^{147}Sm-^{143}Nd chronometer is commonly applied to date both carbonatite dikes and REE mineralization (bastnäsite and monazite) given their enrichment in samarium (Sm) and neodymium (Nd) (*19*). The half-life of ^{147}Sm is 106 billion years (Ga); hence the increase of ^{143}Nd from radiogenic decay is insignificant. For samples with a ^{147}Sm/^{144}Nd ratio of 0.04, such as the bastnäsite and monazite from Bayan Obo, the radiogenic increase in ^{143}Nd/^{144}Nd is 0.0003 and 0.0001 after 1320 and 430 Ma, respectively (Fig. 5A), highlighting the importance of accurate and precise measurements. We use reference materials of monazite (Namaqualand and Iveland) and bastnäsite (K9 and MAD) to assess the quality of published ^{147}Sm-^{143}Nd data from Bayan Obo. The reproducibility of ^{143}Nd/^{144}Nd data (*20*–*22*) for the reference materials (Fig. 5A) is ~0.0002, demonstrating that bastnäsite and monazite with low ^{147}Sm/^{144}Nd ratios are not suitable for radiometric dating when analytical uncertainties are fully considered (Fig. 5, B and C).

To apply ^{147}Sm-^{143}Nd chronometer at Bayan Obo, samples with higher ^{147}Sm/^{144}Nd ratios must be used. When apatite with a ^{147}Sm/^{144}Nd ratio of >0.1 is included, most data show a 430 Ma isochron reference line trajectory (Fig. 5B), with the remaining samples falling between the 1320 and 430 Ma isochron reference lines (Fig. 5B). To this end, we emphasize that the traditional view asserting the REE at Bayan Obo originated at 1320 Ma, without any contribution from the 430 Ma event, is incorrect [e.g., (*20*, *23*)].

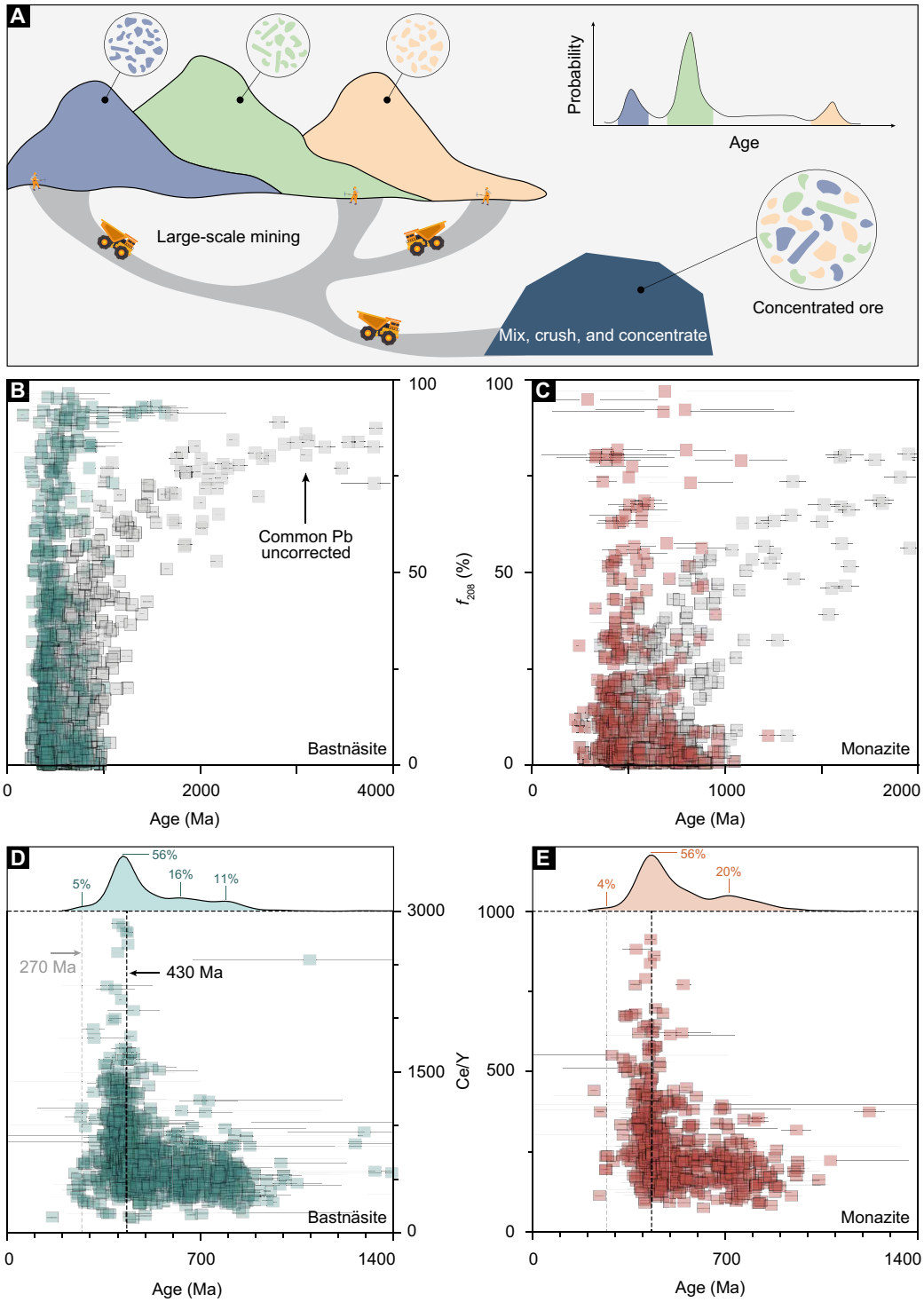

Fig. 4. Using bastnäsite and monazite from concentrated ore samples to constrain timing of mineralization. (**A**) Analogous to detrital mineral provenance studies, concentrated ores from long-term mining best represent the cumulated distribution of metal endowment at Bayan Obo. Common Pb as a function of Th-Pb dates of bastnäsite (**B**) and monazite (**C**) with/without common Pb corrections. Dates with and without common Pb correction are shown as colored and gray symbols, respectively. Without common lead correction, the Th-Pb dates are skewed to much older ages (showing large ranges from ~250 to ~4000 Ma for bastnäsite and from ~250 to ~2000 Ma for monazite). The ^{232}Th-^{208}Pb dates versus Ce/Y ratios of bastnäsite (**D**) and monazite (**E**) from concentrated ores sampled over a 12-year mining history. Uncertainties of ^{232}Th-^{208}Pb dates are plotted at the 1σ uncertainty level. Probability density plots of ^{232}Th-^{208}Pb dates are shown at the top of (D) and (E). The vertical dashed line marks 430 Ma when most dates are clustered with a sharp increase in Ce/Y elemental ratios.

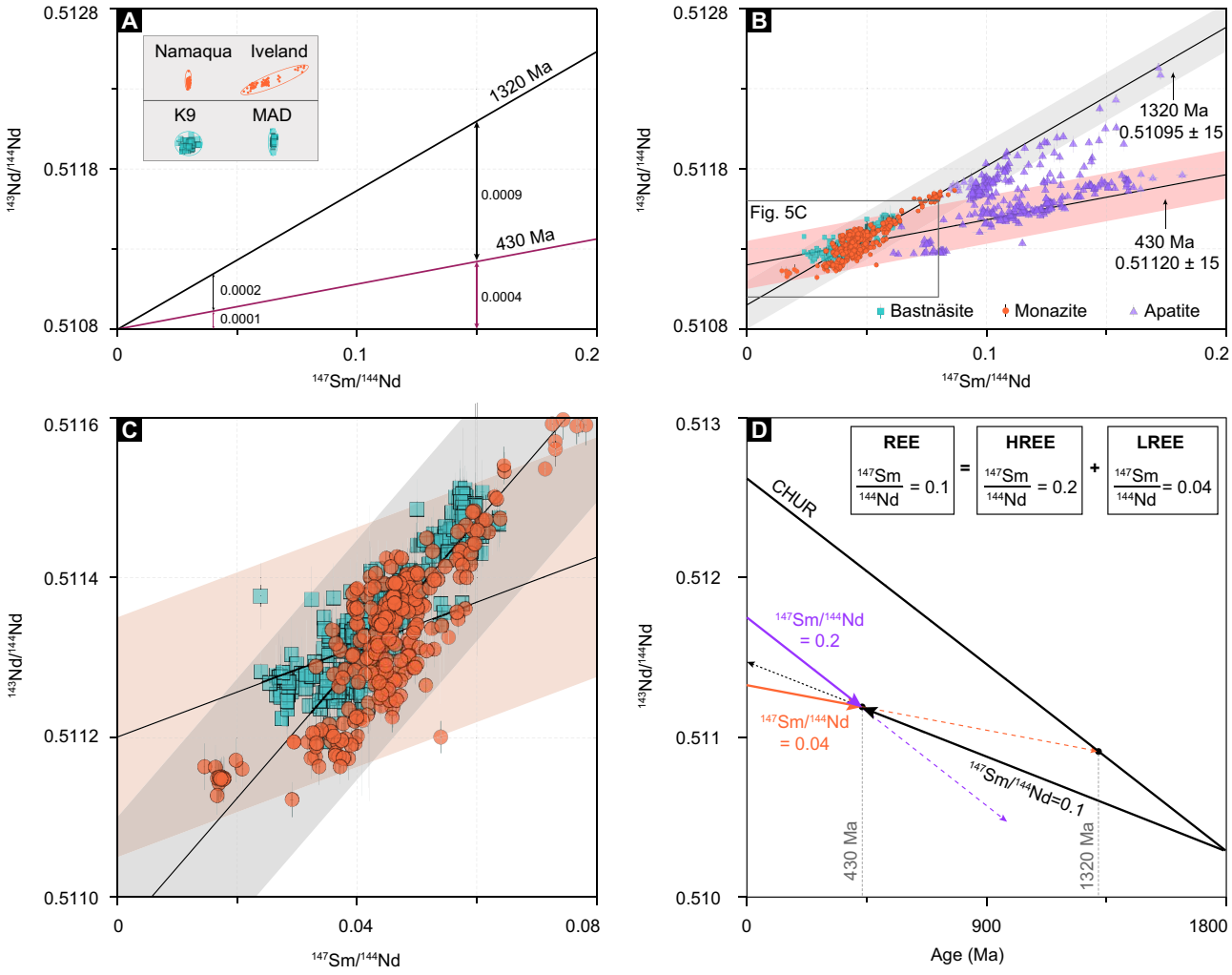

Fig. 5. A compilation and reinterpretation of ^{147}Sm–^{143}Nd isotope data for Bayan Obo samples. The data are from multiple samples with sources being given in supplementary data S6. (**A**) Radiogenic increase in ^{143}Nd/^{144}Nd for samples with different ^{147}Sm/^{144}Nd ratios at 1320 and 430 Ma. The reproducibility of ^{147}Sm-^{143}Nd analysis is evaluated by reference materials: Namaqua and Iveland for monazite and K9 and MAD for bastnäsite (*20*–*22*). The absolute values of reference materials are shifted without modifying their relative variation for comparison. The correlation for Iveland reference material is controlled by its high ^{147}Sm/^{144}Nd ratios (0.2622 to 0.2874). With a reproducibility of 0.0002 for ^{143}Nd/^{144}Nd, samples with low ^{147}Sm/^{144}Nd ratio (<0.08) are not ideal for ^{147}Sm-^{143}Nd dating. (**B**) Rather than uniquely defining a 1320 Ma isochron, the ^{147}Sm-^{143}Nd isotope data show an affinity to a 430 Ma isochron reference line. (**C**) ^{147}Sm-^{144}Nd data of bastnäsite and monazite from Bayan Obo. Reproducibility of the reference materials explains most of the observed variations. Because of limited radiogenic growth of ^{143}Nd/^{144}Nd and poor reproducibility of in situ analysis, bastnäsite and monazite from Bayan Obo cannot differentiate between the 1320 and 430 Ma isochron reference lines. (**D**) Evolution of εNd for minerals with different ^{147}Sm/^{144}Nd ratios. We should only project εNd back to the age of mineral crystallization using measured mineral ^{147}Sm/^{144}Nd ratios. Projection beyond that age needs to consider the fractionation between LREE and HREE. If LREE (e.g., ^{147}Sm/^{144}Nd = 0.04) dated at 430 Ma lies on an evolution line intersecting Chondritic Uniform Reservoir (CHUR) at 1320 Ma, then HREE (e.g., ^{147}Sm/^{144}Nd = 0.2) fractionated from LREE at 430 Ma should intersect CHUR at a much older age, which is not consistent with the remobilization model.

Using εNd as a proxy to decipher the source of REE requires (i) accurate and precise measurements of ^{147}Sm-^{143}Nd isotope data and mineralization age and (ii) calculating εNd only to the age of mineral crystallization (*19*). The positive correlation between calculated εNd and ^{232}Th-^{208}Pb dates from previous studies is best explained by an incorrect utilization of dates beyond mineral crystallization ages (Fig. 5D), rather than a continuous mineralization and/or remobilization lasting for 1 Ga (*14*). Once the mineralization age is defined, the interpretation of εNd also needs to consider the fractionation between LREE and heavy-REE (HREE) (Fig. 5D). If we assume that LREE was formed at 430 Ma by remobilizing the 1320 Ma mineralization, which has an evolution line intercepting Chondritic Uniform Reservoir (CHUR) at 1.3 Ga, then HREE must follow a much steeper evolutional line and intercept CHUR with an older age (≫1.3 Ga; Fig. 5D). To summarize, the remobilization model based on ^{147}Sm-^{143}Nd data only focuses on LREE and fails to balance the fractionation between LREE and HREE.

Bastnäsite and monazite at Bayan Obo are typically U-poor (mode < 0.1 ppm) with mode Th contents of 300 and 1300 ppm, respectively (fig. S11). These low U contents are not ideal for U-Pb dating. While the Th contents are measurable, they are 10 to 1000 times lower than those from other localities (fig. S11). Moreover, bastnäsite

and monazite from Bayan Obo contain high common Pb (defined as f_{208}%) with a mean of 22 and 15%, respectively (Fig. 4, B and C). Together with a long half-life of 14 Ga for ^{232}Th, accurate and precise ^{232}Th-^{208}Pb dating at Bayan Obo is challenging.

Using a ^{232}Th-^{208}Pb isochron approach, which can obtain the common Pb isotope composition and age simultaneously, magnetic fractions of monazite gave dates ranging from 398 ± 10 to 555 ± 11 Ma with a weighted mean of 424 ± 6 Ma (*7*). The common Pb isotope composition of these samples is highly variable with a weighted mean ^{208}Pb/^{204}Pb ratio of 34.22 ± 1.26 (*7*), being lower than that (37.84) predicted by the terrestrial lead isotope evolution model (*24*). This legacy study (*7*) reinforces our conclusion that common Pb must be considered for ^{232}Th-^{208}Pb dating at Bayan Obo.

For bastnäsite and monazite ^{232}Th-^{208}Pb dates obtained by in situ analytical methods, they exhibit a continuous distribution between ~1.4 and ~0.27 Ga with major peaks at 1.3 to 1.4, 0.6 to 0.8, and 0.4 to 0.5 Ga (*6*, *12*, *23*). Critically, these studies commonly assume no common Pb [e.g., (*20*)], which biases the dates to older values.

The U-Pb chronometer is powerful to assess the impact of open-system behavior (i.e., Pb loss) and to correct common Pb (*25*, *26*). However, early zircon U-Pb dating attempts to the H8 unit are unsuccessful (*27*, *28*), and only recovered detrital zircons from nearby gneisses and sandstones (*29*). Further studies consistently show that zircons are related to carbonatites and REE mineralization at Bayan Obo are U-poor; hence, only ^{232}Th-^{208}Pb dates were reported (*16*, *26*). Zircon megacrysts (200 to 700 μm) with a distinctive core-rim texture recovered from banded ores in the east open pit yielded ^{232}Th-^{208}Pb dates of 1325 ± 60 Ma for the core and 455 ± 28 Ma for the rim, which were interpreted as the timing of carbonatite emplacement and hydrothermal overprinting, respectively (*30*). The presence of Mesoproterozoic carbonatites at Bayan Obo is further supported by ^{232}Th-^{208}Pb dates of zircons of ca. 1.3 Ga from a carbonatite dike ~1.5 km southeast of the east open pit (*31*) and banded ores in the east open pit (*32*). More recently, zircons with a bipyramidal morphology were identified in a Fe-rich carbonatite sample from the east end of the west open pit, yielding a ^{232}Th-^{208}Pb date of 435 ± 5 Ma (*33*). This finding has been used to argue for the presence of Paleozoic carbonatite magmatism; however, its contribution to REE has been considered negligible (*33*).

The multi-stage magmatic-hydrothermal history at Bayan Obo is evident, as highlighted by field observations (Fig. 2 and figs. S1 and S2) and the dissolution and recrystallization textures of minerals being dated (*16*, *30*), such as zircon, bastnäsite, and monazite. Hence, further geochronology must consider the potential impact of mixing multistage mineral domains and open-system behaviors. Based on field observations at Bayan Obo, here, we use (i) SIMS zircon U-Pb petrochronology to date carbonatites and (ii) bastnäsite and monazite ^{232}Th-^{208}Pb dating of concentrated ores and pyrite ^{187}Re-^{187}Os dating of vein-type REE ore to constrain the timing of REE mineralization.

430 Ma carbonatite at Bayan Obo

Our zircon U-Pb petrochronology confidently constrains the timing of carbonatite emplacement and associated fluid activities. Zircon U-Pb dates for the H8 unit and the Wu dike precisely date the Mesoproterozoic carbonatites at ca. 1320 Ma (Fig. 3, A and B). These dates are coeval with the Mesoproterozoic zircon ^{232}Th-^{208}Pb dates for carbonatite dike ~1.5 km southeast of the east open pit (*31*) and banded ore from the east open pit (*30*), reinforcing the consensus that Mesoproterozoic carbonatites are abundant at Bayan Obo (*8*, *10*).

The pit wall (west open pit) dated at 430 Ma (Fig. 3C) exhibits extensive alteration with locally distributed Fe and REE mineralization and has been mapped as part of the H8 unit in previous studies. Our successful application of the zircon U-Pb chronometer does not support the notion that dates younger than 1320 Ma are caused by disturbance of the isotopic system [e.g., (*20*)].

The presence of Paleozoic carbonatite with brines and/or alkaline fluids is supported by texture evidence of dated zircons: Zircon cores have clear patched or oscillatory zoning (Fig. 3, D and F), whereas rims contain alteration assemblages including apatite, ankerite (Fig. 3C), and mica and amphibole veins (Fig. 3E), which are consistent with zircons crystallizing from carbonatitic melts with the presence of brines and/or alkaline fluids.

Carbonatitic systems typically evolve from Ca-rich to Mg-rich melts (*34*). Field observations reveal that many coarse-grained dikes are Ca-rich (e.g., fig. S2, B and E) and cut the Mg-rich rocks within the H8 unit (*18*). Such a crosscutting relationship is consistent with a younger age of the Ca-rich dikes dated at 430 Ma ago. Previous models propose that the coarse-grained dikes are early phases of the Mesoproterozoic carbonatites (*13*) with an evolutional trajectory from Mg- to Ca-rich melts (*12*), which conflict with crosscutting relationships at Bayan Obo and the evolutional trend of carbonatitic melts in general. Remelting Mesoproterozoic carbonatites at ~440 and ~270 Ma is also proposed for the coarse-grained carbonatites (*35*), but high-temperature assemblages formed during remelting are yet to be found, and this model fails to explain the temperature gradient required to remelt carbonatites at shallow levels.

With numerous zircons being dated at ca. 430 Ma across the entire Bayan Obo area (n = 75; Fig. 3), we provide robust geological and chronological evidence for the presence of Paleozoic carbonatites. Misinterpreting the ca. 430 Ma carbonatites as part of the Mesoproterozoic H8 unit unlikely is limited to the dated pit wall in the west open pit (Fig. 3C). The Mg-rich nature of the 430 Ma Wang dike (fig. S8) also invalidates the use of Mg/Ca ratio as a proxy for distinguishing between Mesoproterozoic and Paleozoic carbonatites. We emphasize that mapping the distribution of Paleozoic carbonatites is critical for future studies.

Age of REE mineralization and metal contribution from the Paleozoic carbonatites

In addition to mineralization age, constraining the contribution of metal endowment from each stage is fundamental for a coherent genetic model. Given the known heterogeneity and multistage history of REE mineralization at Bayan Obo (*16*), using samples from limited outcrops could be biased by samples from a certain mineralization stage as documented previously (Fig. 2D). To overcome this pitfall, here, we use concentrated ores from large-scale and long-term mining, a methodology analogous to detrital mineral provenance studies (Fig. 4A), for a statistical assessment.

Without the knowledge of Paleozoic carbonatites, previous studies prefer a dominant role of Mesoproterozoic carbonatite on REE mineralization. This model requires that the majority of Mesoproterozoic REE minerals were remobilized. The apparent correlation between total Pb contents and ^{232}Th-^{208}Pb dates of bastnäsite and monazite is used as a key argument (*20*). However, for a set of samples with negligible U and variable ^{232}Th-^{208}Pb dates, the total Pb budget is dominated by radiogenic ^{208}Pb, which is a function of ^{232}Th-^{208}Pb dates.

For this reason, a correlation between total Pb contents and ^{232}Th-^{208}Pb dates can be predicted mathematically (fig. S18); hence, the previous argument of Pb loss based on this correlation is incorrect (*20*).

We have already demonstrated the presence of Paleozoic-aged carbonatites; hence, the dominant peak of ^{232}Th-^{208}Pb dates at ca. 430 Ma may represent a major stage of REE mineralization. A Paleozoic REE mineralization event is further supported by (i) our 431 ± 3 Ma Re-Os pyrite isochron age from the vein-type REE mineralization (fig. S17), (ii) monazite Th-Pb isochron dating at ca. 430 Ma (*7*), and (iii) Sm-Nd data's affinity to the ca. 430 Ma isochron reference line (Fig. 5B).

A mineralization age of ca. 430 Ma gives a εNd of −16 (Fig. 5), which implies a crustal source of REE, being consistent with the radiogenic nature of the initial ^{187}Os/^{188}Os composition of vein-pyrite (0.52 ± 0.09; fig. S17) and a zircon εHf of approximately −5 (*33*).

In our two-stage REE mineralization model, ^{232}Th-^{208}Pb dates falling between ca. 1320 and ca. 430 Ma are best explained by mixing Mesoproterozoic and Paleozoic mineral grains. Assuming Th contents for Mesoproterozoic and Paleozoic grains have a ratio of 1:3, then, the 44% mixed grains with ^{232}Th-^{208}Pb dates peaking at 630 to 780 Ma (Fig. 4, D and E) imply a mixing ratio of 6:4. This is equivalent to a REE contribution of 72% from the Paleozoic-aged carbonatites, a dominant role being ignored in previous studies. The Th content ratio of 1:3 likely is underestimated, and the REE contribution of ~70% from Paleozoic carbonatites represents a minimum estimate.

Vein-type REE mineralization is volumetrically minor, with a dominant peak of ^{232}Th-^{208}Pb dates of concentrated ores at 430 Ma, requiring that a majority of ^{232}Th-^{208}Pb dates from the banded ores are ca. 430 Ma. This can be explained by deposition of REE minerals at ca. 430 Ma along the bedding of the H8 unit via metasomatism by brines and alkaline fluids exsolved from the Paleozoic carbonatites. Critically, the presence of undeformed mineralization along bedding provides strong support that at least a portion of, and possibly most banded ores were formed by metasomatism at ca. 430 Ma (see below for further discussion).

A small portion of ^{232}Th-^{208}Pb dates (<5%) clusters at 270 Ma, isochronous with the emplacement of Permian granites (*9*), which has a negligible impact on REE mineralization but could be important for coarse-grained and high-grade Nb mineralization (*26*, *36*).

Hydrothermal controls of REE mineralization from the Paleozoic carbonatites

With the timing of carbonatites and mineralization being firmly constrained, we explore the mechanisms controlling REE mineralization using trace elements of bastnäsite and monazite. The Ce/Y elemental ratio, an index of fractionation between LREE and HREE, increases sharply at ca. 430 Ma (fig. S15). Previous studies argue that grains dated at ~430 Ma formed from remobilizing the ~1320 Ma REE mineralization. If this is the case, then the Ce/Y increase indicates a preferential enrichment of LREE during remobilization, and the residual HREE is expected within the H8 unit, which is not reported. To this end, the increase in Ce/Y ratios reinforces our model that REE mineralization at ca. 430 Ma was from a different source rather than recycling Mesoproterozoic mineralization.

The mineral assemblages of hydrothermal alteration within the H8 unit, carbonatite dikes, and country rocks (*8*, *37*) and fluid inclusion studies (*38*, *39*) all emphasize carbonatitic brines and alkaline fluids as a controlling factor for REE mineralization. Experimental studies reveal that transportation of LREE is enhanced by alkaline fluids at lower temperatures (*40*, *41*), whereas HREE preferentially precipitate when alkaline fluids react with Si-rich rocks—a process known as fenitization (*42*). Silicon-rich rocks such as sandstone, quartzite, and gneiss are abundant at Bayan Obo, and this provides an ideal environment for brine/fluid-rock interaction upon carbonatite emplacement, as evidenced by extensive fenitization (*8*, *37*).

We concur with the previous model that the Mesoproterozoic carbonatites erupted effusively into a nearby basin with coeval deposition of clastic rocks (*8*) and emplacement of carbonatite dikes. This eruptive model (Fig. 6A) neatly explains the stratiform morphology and diversity in structure and geochemistry of the H8 unit, such as banded textures, occurrences of detrital quartz, interbedded clastic rocks, and carbon and oxygen isotopes compositions of both igneous and sedimentary affinity (*4*, *5*, *8*, *16*). The eruptive nature of Mesoproterozoic carbonatites hindered magma fractionation. Therefore, metal enrichment in brines/fluids is prohibited (*43*), and REE mineralization is low grade and disseminated (Fig. 6A). This does not exclude the presence of high-grade ore with an age of 1320 Ma at local scales, both within the H8 unit and associating carbonatite dikes (e.g., the Wu dike; fig. S5). Although REE from this stage only is <30%, it provides an excellent lithology for further metasomatic reactions (*40*), especially when the permeability of Mesoproterozoic carbonatites was enhanced by deformation (Fig. 6B). A dominant REE contribution from the Paleozoic carbonatites also allows that a portion of banded ores were formed at 1320 Ma, which were deformed later.

The presence of abundant dikes dated at ca. 430 Ma ago and emplaced at shallow levels suggests the presence of Paleozoic carbonatites at depth (Fig. 6C), which would release brines and alkaline fluids rich in REE upon cooling and crystallization. During migration and ascent, the brines and fluids reacted with Si-rich country rocks (Fig. 6D) with a preferential deposition of HREE through fenitization (*42*). The residual brines/fluids became LREE enriched and precipitated LREE via metasomatic reactions with the H8 unit (*5*, *16*, *40*), both as veins and along the bedding (Fig. 6E). This stage contributed more than 70% of the REE endowment. Mineralization along bedding is largely undeformed but inherits the deformation pseudomorph (e.g., folding and fish microstructures) of the H8 unit (Fig. 6E), supporting our metasomatism model.

The above model predicts that HREE were enriched in the deeper parts of Bayan Obo through fenitization (Fig. 6D). Worldwide carbonatites have an average LREE/HREE ratio of ~10 (*44*), with 100 million Mt of LREE being deposited at shallow levels, a simple mass balance calculation suggests that HREE resource deposited through fenitization at depth could reach 10 million Mt. HREE enrichment has been found at depth through drilling (*45*). This HREE heritage should be considered when deciphering the sources of REE and in future exploration and mining activities.

Outlook and implications

Revealing the presence of ca. 430 Ma carbonatites at Bayan Obo only is a start, and many questions remain to be answered. Through integrating geological mapping and petrochronology, future studies focusing on the distribution of Paleozoic carbonatites and associated alkaline intrusive complexes are fundamental for ore genesis, mineral exploration, and mining. A crustal affinity in Os-Nd-Hf isotopes [Fig. 5 and fig. S17; (*33*)] for the Paleozoic carbonatites, and by inference the REE mineralization, is in contrast with many carbonatites showing a mantle isotopic affinity. Global carbonatites show an increase

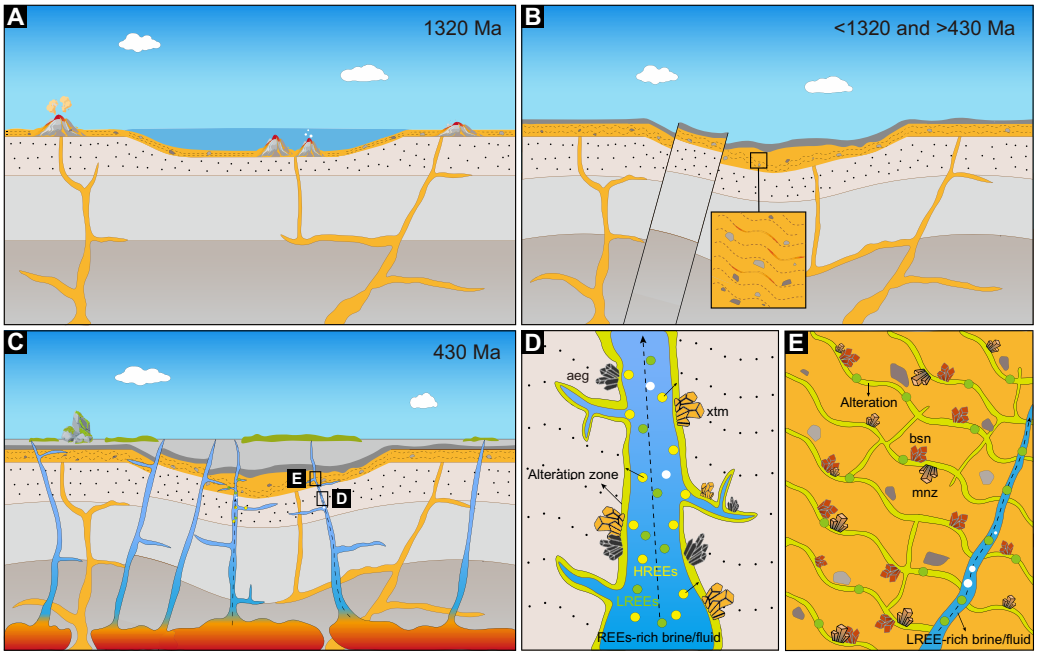

Fig. 6. An integrated genetic model for Bayan Obo. (**A**) Effusive eruption of carbonatitic magmas into a basin at ca. 1320 Ma ago with potential associated deposition of limestone and clastic rocks, forming the H8 unit. Mineralization at this stage is low grade and disseminated due to limited magmatic fractionation and metal enrichment in brines/fluids. (**B**) H8 unit was deformed resulting in an increase in its permeability—ideal for later metasomatism by carbonatitic brines and alkaline fluids. (**C**) Voluminous carbonatitic magmas emplaced beneath Bayan Obo at ca. 430 Ma ago, with abundant dikes intruding the H8 unit and country rocks at the surface. After extensive crystallization and fractionation, brines and alkaline fluids rich in REE exsolved from the Paleozoic carbonatites at depth. (**D**) During upward migration, the brines/fluids lost their HREE via reaction with Si-rich rocks (i.e., xenotime and aegirine). (**E**) Once reached shallow levels, the residual brines/fluids rich in LREE reacted with the H8 unit, resulting in efficient precipitation of REE through metasomatism as veins and along beddings [i.e., bastnäsite (bsn) and monazite (mnz)]. Minimum REE contribution at this stage is estimated at 70%.

in initial $^{87}Sr/^{86}Sr$ isotopes through time, which was linked to an increase in subduction flux to the mantle (*46*). The young carbonatites we identified here then is expected to have radiogenic Sr isotopes, and a crustal affinity in Os-Nd-Hf isotopes. The fractionation between LREE and HREE has significant implications for ore-forming processes and the interpretation of Sm-Nd data, highlighting the importance of considering these effects in future studies. For the H8 unit, while an eruptive carbonatite origin in the Mesoproterozoic carbonatites is attractive, local presence of sedimentary carbonates is highly possible. An improved understanding on the petrogenesis of multistage carbonatites will help reveal the controls of this world-class REE deposit.

The two-stage model we proposed here emphasizes the role of metasomatism, with its efficiency being promoted when permeability of the first-stage carbonatite was enhanced by deformation. It is generally assumed that banded ores were formed earlier, followed by deformation, and the vein-type ores were later and undeformed. However, REE-bearing fluorite and pyrite veins along bedding without deformation also are not uncommon (fig. S1B). An attractive scenario is that the primary H8 unit was deformed, and a portion of banded ores were introduced later by brines/fluids along banding, inheriting the pseudomorph of microstructures via metasomatism. Further studies are required to fully explore the origin of banding and the role of deformation on REE mineralization at Bayan Obo and similar deposits globally.

Our concentrated ore approach provides a framework to understand metal contribution through time. Paragenetic constrained samples will offer further details on the enrichment process of metals from each stage, and/or potential redistribution and re-enrichment of existing mineralization by later stage magmatic-hydrothermal activities.

In addition to REE, Bayan Obo is initially found as a Fe deposit and contains considerable resources of F, Nb, and potentially Sn as by-products (*47*, *48*). Iron rich carbonatites are rare, and at Bayan Obo, REE is the by-product of Fe mining, which is the main reason why this deposit is economically valuable with low cost. While carbonatites are central for metal enrichment, the Permian granites also have played a significant role in forming high-grade Nb mineralization (*26*, *36*). In comparison to REE, other resources such as Fe and Nb have received much less attention. A coherent genetic model is warranted to decipher the controlling factors of all metals.

Carbonatites are rare in space and deep time, but the presence of multiple stages of carbonatites at one locality is not unique. In addition to Bayan Obo, repeated occurrence of carbonatites has been documented in a few places globally (*49*). Failing to identify the later stage, ore-fertile carbonatite could be common pitfalls without careful field work, robust petrochronology, and correct interpretation of isotope data. Taking the Miaoya REE deposit, China as an example, REE mineralization dated at ca. 240 Ma is significantly younger than the ca. 440 Ma ore-hosting carbonatite and syenite (*50*). Since the ca. 440 Ma carbonatite unlikely can sustain mineralization 200 Ma later, it's possible that the ore-fertile carbonatite has not been identified and thus requires further investigation to accurately evaluate the deposit genesis.

Our study highlights that robust deposit geology and accurate geochronology are paramount requirements into decoding and contextualizing the controlling factors for ore formation. Our two-stage model is readily applicable to other deposits, and future exploration should focus on regions where efficient metasomatism is driven by carbonatitic brines and alkaline fluids.

MATERIALS AND METHODS

Experimental design

Timing of carbonatites and mineralization is central to the genetic debates at Bayan Obo (Fig. 2D). To obtain accurate and precise timing constraints and interpret isotopic dates without ambiguity, it is critical to distinguish the differences between dates and ages. This requires (i) sampling under a robust geological framework; (ii) a thorough understanding of geochronology, with an emphasis on the strength and weakness of the isotope system being used/discussed; and (iii) correct isotopic analysis and data reduction.

Given the extensive dating approaches applied to Bayan Obo, the concerns on open system behaviors and mixing multistage mineral domains, and the challenges in estimating the contribution of metal endowment from each mineralization stage, here, we have (i) discussed the strength and weakness of main radiometric isotope systems applied to Bayan Obo; (ii) applied zircon U-Pb petrochronology to evaluate the impact of open system behaviors and to constrain the timing of carbonatite emplacement; and (iii) used concentrated ore samples to obtain a representative dataset on mineralization ages.

Deposit geology of Bayan Obo

The Bayan Obo REE deposit differs from typical carbonatite related REE deposits for its enrichment in Fe mineralization (Fig. 2, B and C), and without well-defined exposure of cogenetic silicate rocks (*16*, *26*, *36*). Massive magnetite ores mostly occur in the core of the main and east open pits and, to a lesser extent, as small clusters in the west open pit, which are surrounded by banded REE ores (Fig. 2, B and C; *51*, *52*).

Although the H8 dolomite was and is still used throughout the literature, here, we suggest using H8 unit instead of H8 dolomite mainly for three reasons, (i) its origin and evolution are debated (Fig. 2D), but dolomite refers to sedimentary carbonate when used as a rock name and (ii) its composition is not homogenous with the presence of calcium and iron rich carbonatites (*3*) and (iii) the presence of multistage carbonatites.

The H8 unit and country rocks are crosscut by more than 60 carbonatite dikes (*53*), some of which were misinterpreted as carbonate xenoliths (Fig. 2, B and C, and fig. S2). These dikes are represented by coarse-grained Mg-rich dikes in the west and main open pits (fig. S2, A and C) and Ca-rich dikes in the east contact zone (figs. S2, D and E, and S9).

Fenitization comprising amphibole and aegirine, which is a typical alkaline metasomatism, is commonly associated with the carbonatite dikes (fig. S2, A and E) and high-grade Fe and REE ores (*37*). Mining and deep drilling also revealed fenitization in the quartzite and slate country rocks beneath the H8 unit (*54*).

The bands mainly consist of dolomite, calcite, bastnäsite, monazite, fluorite, magnetite, and apatite (fig. S1, A and B) and are crosscut by vein-type mineralization bearing bastnäsite, monazite, fluorite, apatite, pyrite, and barite (fig. S1, B and D). While the bands show clear textures of foliation and/or deformation (folding and fish microstructures; fig. S1, A to D), the timing between deformation and REE mineralization along bedding is unconstrained (*5*). The presence of undeformed mineralization along bedding suggests that at least a portion of mineralization is post-deformation and inherits pseudomorph of deformation. The coarse-grained carbonatites and vein-type ore are not deformed (fig. S1D).

Permian granites dated at 270 Ma (*36*) with associated skarn mineralization are voluminous in the east contact zone (Fig. 2, B and C) and occur as felsic dikes throughout the mining area (figs. S2B and S4B). Previous geological mapping inferred that Permian granites are ubiquitous beneath Bayan Obo (*9*).

Carbonatite samples

Sample EB130-2 was collected from the H8 unit on the eastern side of the east open pit. This ore-hosting carbonatite outcrop has been intruded by post-ore diabase dikes and felsic dikes (fig. S4, A and B). The hand specimen is a massive mica-altered carbonatite, primarily composed of calcite (55%; fig. S4C), mica veins (30%; fig. S4E), and minor light-green acicular riebeckite (fig. S4F), with some calcite grains containing dense punctate black magnetite (10%; fig. S4D). Zircons in this sample are light brown and transparent, appearing as euhedral tetragonal bipyramids of 100 to 200 μm. The zircons exhibit faint and broad zoning in cathodoluminescence (CL) images (fig. S4G).

Sample EB170 was collected from a 1.5-m–wide carbonatite dike (Wu dike) in the east contact zone. The Wu dike intruded into a quartz conglomerate, triggering fenitization at the contact zone (fig. S5, A and B). Petrographic analysis shows extensive REE mineralization, with REE minerals (bastnäsite) comprising up to 40% of the sample at a local scale. In addition, the sample contains calcite (15%) and strontianite (30%), along with minor quartz (8%) and barite (5%) (fig. S5, C and D). The zircon grains within the sample are milky yellow and range from 40 to 80 μm in size. CL imaging predominately shows chaotic and fragmented patterns, with some grains exhibiting well-defined, fine concentric zoning at their edges (fig. S5E).

Sample EB21-14 was obtained from a weathered yellowish-brown carbonatite cliff situated on the southwest side of the west open pit. This carbonatite outcrop has been intruded by several post-ore felsic dikes (fig. S6A). The carbonatite sample (EB21-14) is massive, mostly composed of coarse-grained calcite (90%; fig. S6, B and D) and minor apatite (8%; fig. S6C). The cleavage planes of the coarse-grained calcite are filled with yellowish-brown iron staining (fig. S6, B and D). Zircons in this sample are subhedral to euhedral tetragonal bipyramids of 50 to 100 μm and mainly display patchy and blurry zoning in CL images (fig. S6E).

Samples EB21-06 and EB21-36 were collected from a grayish-white carbonatite dike located on the western side of the west open pit. This dike spans ~60 m in width, with blue-green and dark brown alkaline alteration on both sides (fig. S7A). The carbonatite sample EB21-06 is massive and composed mainly of coarse-grained dolomite (50%) with interstitial space filled with fine-grained dolomite (15%), apatite (15%), and monazite and bastnäsite (15%; fig. S7, B and D). Sample EB21-36 is mainly composed of coarse-grained dolomite (80%) crosscut by some fine-grained Sr and Ba-rich carbonate veinlets (10%; fig. S7, C and E), monazite, and bastnäsite (5%; fig. S7, D and E), as well as mica and riebeckite (5%) along the grain boundaries (fig. S7, C and D). Zircons from this dike exhibit subrounded pyramidal morphology of 40 to 80 μm. Some zircons display fine growth zoning, whereas others show chaotic and patchy zonation in CL images (fig. S7F).

Sample EB103B was collected from a carbonatite dike located on the south side of the main open pit. This dike spans ~100 m in width and extends outward in a V-shaped pattern (fig. S8, A to C). Although it appears grayish white, resembling fresh carbonatite to the naked eye, thin-section observation reveals varying degrees of alkaline alteration, particularly in the alteration of riebeckite and mica (fig. S8, E to G). We name this dike as Wang dike after K.-Y. Wang, who has devoted her career to Bayan Obo for ~60 years. Sample EB103B is mainly composed of dolomite (80%; fig. S8D), light-green clustered riebeckite (10%), and minor mica (3%), sphalerite, and pyrite (5%). Zircons from this sample range in size from about 30 to 50 μm, characterized by prismatic cores with clear and patchy zonation, as well as subrounded, chaotically, and blurry zoned rims in CL images (fig. S8H).

Samples EB21-57 and EB21-58 were collected from a 3-m-wide and 1-m-wide carbonatite dikes in the east contact zone (fig. S9, A and B), respectively. The dikes are primarily composed of calcite but in many areas have undergone alteration, iron staining, and weathering (fig. S9B). In the thin-section sample, EB21-57 shows interlocking calcite (80%) up to 5 mm in size. Variable degrees of iron staining occur along the calcite cleavage planes (fig. S9C), with planes exhibiting fine-grained quartz and barite aggregates (15%; fig. S9D). Sample EB21-58 is mainly composed of calcite (75%) and riebeckite (15%; fig. S9E) with minor quartz (3%; fig. S9F). The alignment of columnar riebeckite along the calcite boundary caused the entire section to exhibit a unidirectional orientation, with minor veinlets of magnetite and limonite (7%). The two dikes are close with each other with limited yield of zircons and hence are pooled together for further analysis. Zircons in this sample range in size from 50 to 100 μm, displaying subrounded prismatic shapes with sector zones or with fine concentric growth zones in CL image (fig. S9G).

Concentrated ores

To ensure a close resemblance to the distribution of metal endowment at Bayan Obo (i.e., how many grains are 1320 or 430 Ma), we sampled four concentrated REE ores (mainly bastnäsite and monazite) spanning a ~12-year mining history, namely, EB2009, EB2012, EB2016, and EB2020.

Sample EB2009 consists mostly of bastnäsite (56%) and monazite (23%), with trace proportions of fluorite (5%), iron oxides (4%), apatite (2%), aegirine (2%), calcite (1%), and ankerite (1%). The bastnäsite and monazite crystals are anhedral of 20 to 80 μm and 20 to 50 μm, respectively (fig. S10).

Sample EB2012 consists mostly of bastnäsite (62%) and monazite (21%), with trace proportions of apatite (5%), fluorite (4%), iron oxides (3%), aegirine (1%), and ankerite (1%). The bastnäsite and monazite crystals are anhedral of 20 to 50 μm and 20 to 50 μm, respectively (fig. S10).

Sample EB2016 consists mostly of bastnäsite (61%) and monazite (25%), with trace proportions of iron oxides (3%), apatite (3%), fluorite (3%), and cerussite (1%). The bastnäsite and monazite crystals are anhedral of 20 to 100 μm and 20 to 50 μm, respectively (fig. S10).

Sample EB2020 consists mostly of bastnäsite (45%) and monazite (27%), with trace proportions of fluorite (2%), iron oxides (2%), and apatite (2%). The bastnäsite and monazite crystals are anhedral and contain 20 to 50 μm and 20 to 50 μm, respectively (fig. S10).

Analytical methods

SIMS zircon U-Pb dating

Zircon U-Pb dating was performed using a CAMECA IMS-1280HR ion microprobe at the Institute of Geology and Geophysics, Chinese Academy of Sciences following Li *et al.* (*55*). The O_2^- primary ion beam was accelerated at 13 kV, with an intensity of ~10 nA. The ellipsoidal spots are 20 μm by 30 μm or 10 μm by 15 μm to accommodate the different sizes of zircons. Positive secondary ions were extracted with a 10-kV potential. The mass resolution of ~5400 (defined at 50% peak height) was used to separate Pb^+ peaks from isobaric interferences. The $^{90}Zr_2{}^{16}O^+$ peak was used as a reference peak for centering the secondary ion beam, and energy and mass adjustments. Each measurement consists of seven cycles and a total analytical time of ~16 min. The 91,500 zircon [1065.4 Ma; (*56*)] was used to calibrate the instrumental mass fractionation, and the TEMORA zircon [417 Ma; (*57*)] was used to monitor data accuracy. The measured Pb isotopic compositions were corrected for common Pb using measured ^{204}Pb, an index for nonradiogenic Pb. We used Pb isotope composition of galena measured in this study instead of following the terrestrial Pb isotope evolution model (*24*) for common Pb correction. Data reduction and age calculation were carried out using the IsoplotR program (*58*). Repeated analyses of TEMORA zircon yield a U-Pb concordia age of 419 ± 2 Ma (2SE, $n = 33$), being identical with the recommended age of 416.8 ± 1.1 Ma (*57*).

TIMS pyrite Re-Os dating

The Re-Os isotope analyses were conducted at the Arthur Holmes Laboratory at Durham University following the analytical protocol of Li *et al.* (*59*) and Selby *et al.* (*60*). Separated pyrites were weighed, spiked with a mixed tracer, and loaded into Carius tubes. The pyrite samples were equilibrated with the tracer solution that contains a known ^{185}Re and ^{190}Os composition and abundance. Samples and tracer solution were digested in 11 N HCl (3 ml) and 15.5 N HNO_3 (8 ml) in a sealed Carius tube at 220°C for 48 hours. Osmium and Re were purified from the acid medium using solvent extraction ($CHCl_3$), microdistillation, and NaOH-acetone solvent extraction and single-bead chromatography methods. Purified Re and Os were then loaded onto nickel and platinum filaments, respectively, with the isotopic measurements conducted using negative thermal ionization mass spectrometry on a ThermoElectron TRITON mass spectrometer. We used a secondary electron multiplier in peak-hopping mode for Os and static Faraday collection for Re. Total procedural blanks for Re and Os were 2.6 ± 0.4 and 1.5 ± 1.6 pg, respectively, with an average $^{187}Os/^{188}Os$ value of 0.21 ± 0.10 (2σ, $n = 5$). All uncertainties are determined by error propagation of uncertainties in Re and Os mass spectrometer measurements, blank abundances and isotopic compositions, spike calibrations, and reproducibility of standard Re and Os isotope values. Data reduction and age calculation were carried out using an inverse isochron approach (*61*).

Laser ablation ICPMS Th-Pb dating and trace element analysis of bastnäsite and monazite

The Th-Pb dating and trace element analysis of bastnäsite and monazite were performed on an Agilent 7900 quadrupole (Q)–inductively coupled plasma mass spectrometry (ICPMS) instrument (Agilent Technologies, USA) in combination with an ArF excimer laser (λ = 193 nm) with a pulse duration of 15 ns (GeolasHD, Göttingen, Germany) at China University of Geosciences, Wuhan. Matrix-matched reference materials (K-9 bastnäsite and USGS-44069 monazite) were used to correct for Th and Pb fractionation and instrumental mass discrimination. The analysis was performed with a spot size of 32 μm.

Each spot analysis involved approximately 20 s of background data acquisition and 50 s of sample data acquisition. Two K-9 and one MAD809 analyses were measured after every five to eight unknown bastnäsite samples. Two USGS-44069 and one Trebilcock analyses were measured after every five to eight unknown monazite samples. We followed the method of Liu *et al.* (*62*) for data reduction. Uncertainties of the calibrated isotope ratios include those from samples, external standards, and deviations from the external reference materials. Repeated analysis of MAD809 bastnäsite and Trebilcock monazite during this study yield Th-Pb ages of 550 ± 21 Ma (2SD, n = 159) and 275 ± 15 Ma (2SD, n = 66), respectively, which are 1 to 5% older than recommended values (520 ± 5 and 272 ± 4 Ma ago; *21*, *63*). Such a drift is well expected considering the compositional diversity of bastnäsite and the reproducibility we can achieve (2 to 5%), highlighting the need of well-characterized reference materials for dating REE minerals with better precision.

Trace element concentrations were calibrated using NIST610 as the external standard material. Each element was expressed as $A(CO_3F)$ for bastnäsite or $A(PO_4)$ for monazite, of which the sum was normalized to 100 weight % (*64*). Isotopic and elemental compositions were calculated using an in-house MATLAB software. For multiple groups of standards, we performed an interpolation of linear fit to ratios for drift corrections. Signal sections of each analysis were checked to avoid inclusions and get a very similar interval for standards and unknowns. Uncertainties for trace element analyses are better than 10 to 15%.

Common lead correction

Monazite Th-Pb isochron dating (*7*) and the common occurrence of galena with REE minerals highlight the occurrence of common Pb with variable lead isotope composition for samples at Bayan Obo. The low Th contents (fig. S11A) of bastnäsite (mode = 300 ppm) and monazite (mode = 1300 ppm) in comparison to those from igneous and metamorphic environments (1000 to 7000 ppm and 3–14 wt%, (*65*, *66*) and extremely long half-life of ^{232}Th (14 Ga) make common lead correction critical for obtaining accurate and precise Th-Pb dates.

Common Pb correction using measured ^{204}Pb is compromised by the low counts of ^{204}Pb, we instead used measured ^{207}Pb as a proxy of common Pb, which is ~15 times higher than ^{204}Pb; hence, more accurate and precise measurements are possible. Using ^{207}Pb as a proxy of common Pb is possible because these samples contain exceptionally low U (<0.1 ppm; fig. S11B); hence, ^{207}Pb from the decay of ^{235}U is negligible. Highly variable isotope composition of common Pb hampers using the terrestrial Pb isotope evolution model of Stacey and Kramers (*24*). We used measured Pb isotope composition of galena collected in the mining area (fig. S13) with a close association with REE mineralization for this purpose, which has an average ^{208}Pb/^{207}Pb ratio of 2.42 ± 0.02 (n = 10).

Following this rigorous procedure of common Pb correction, the average common-lead contents (defined as f_{208}%, which is the ratio of common ^{208}Pb to total ^{208}Pb) of bastnäsite and monazite are 22 and 15%, respectively (fig. S12). This reinforces our conclusion that common Pb correction is critical to obtain accurate and precise ^{232}Th-^{208}Pb dates at Bayan Obo.

Correlation between bastnäsite and monazite Pb contents and ^{232}Th–^{208}Pb dates

For bastnäsite and monazite samples deficient in U, such as the samples at Bayan Obo, their Pb contents are dominated by radiogenic ^{208}Pb (^{208}Pb*) from decay of ^{232}Th. Consequently, a correlation between Pb contents and Th-Pb ages could be predicted mathematically (fig. S18), as the latter is a function of ^{208}Pb* and Th described by the following (Eq. 1)

$$\text{Th} - \text{Pb age} = \ln\left(^{208}\text{Pb}/\text{Th} + 1\right)/\lambda \quad (1)$$

For a set of samples, the degree of this correlation is controlled by the variation in their ages and Th contents (fig. S18). When ages vary significantly, a stronger correlation is expected. In contrast, an increase in the variation of Th contents weakens the correlation (fig. S18). Given this correlation is regulated by radiometric decay, it should not be mistakenly used as evidence of lead loss.

Supplementary Materials

The PDF file includes:

Figs. S1 to S18
Table S1
Legends for data S1 to S9

Other Supplementary Material for this manuscript includes the following:

Data S1 to S9

REFERENCES AND NOTES

1. B. K. Sovacool, S. H. Ali, M. Bazilian, B. Radley, B. Nemery, J. Okatz, D. Mulvaney, Sustainable minerals and metals for a low-carbon future. *Science* **367**, 30–33 (2020).
2. M. Anenburg, S. Broom-Fendley, W. Chen, Formation of rare earth deposits in carbonatites. *Elements* **17**, 327–332 (2021).
3. U. S. Geological. Survey, *Mineral commodity summaries 2024*. (U S. Geological. Survey, 2024); https://pubs.usgs.gov/publication/mcs2024.
4. E. C. T. Chao, J. M. Back, J. A. Minkin, Y. C. Ren, Host-rock controlled epigenetic, hydrothermal metasomatic origin of the Bayan Obo REE-Fe-Nb ore deposit, Inner Mongolia, P.R.C. *Appl. Geochem.* **7**, 443–458 (1992).
5. X. Y. Yang, W. D. Sun, Y. X. Zhang, Y. F. Zheng, Geochemical constraints on the genesis of the Bayan Obo Fe-Nb-REE deposit in Inner Mongolia, China. *Geochim. Cosmochim. Acta* **73**, 1417–1435 (2009).
6. M. X. Ling, Y. L. Liu, I. S. Williams, F. Z. Teng, X. Y. Yang, X. Ding, G. J. Wei, L. H. Xie, W. F. Deng, W. D. Sun, Formation of the world's largest REE deposit through protracted fluxing of carbonatite by subduction-derived fluids. *Sci. Rep.* **3**, 1776 (2013).
7. J. W. Wang, M. Tatsumoto, X. H. Li, W. R. Premo, E. C. T. Chao, A precise ^{232}Th-^{208}Pb chronology of fine-grained monazite: Age of the Bayan Obo REE-Fe-Nb ore deposit, China. *Geochim. Cosmochim. Acta* **58**, 3155–3169 (1994).
8. M. J. Lebas, J. Keller, K. J. Tao, F. Wall, C. T. Williams, P. S. Zhang, Carbonatite Dykes at Bayan Obo, Inner-Mongolia, China. *Mineral. Petrol.* **46**, 195–228 (1992).
9. L. J. Drew, Q. R. Meng, *Geologic map of the Bayan Obo area, Inner Mongolia, China*. (U. S. Geological. Survey, 1990); https://doi.org/10.3133/i2057.
10. X. M. Yang, M. J. Lebas, Chemical compositions of carbonate minerals from Bayan Obo, Inner Mongolia, China: implications for petrogenesis. *Lithos* **72**, 97–116 (2004).
11. D. Lentz, Reexamination of the genesis of the bayan Obo Fe-REE-Nb Deposit: Autometasomatic oxidation of an extremely fractionated ferrocarbonatite. *Acta Geol. Sin.* **88**, 361–363 (2014).
12. K. F. Yang, H. R. Fan, F. Pirajno, X. C. Li, The Bayan Obo (China) giant REE accumulation conundrum elucidated by intense magmatic differentiation of carbonatite. *Geology* **47**, 1198–1202 (2019).
13. X. C. Li, H. R. Fan, J. H. Su, D. I. Groves, K. F. Yang, X. F. Zhao, Giant rare earth element accumulation related to voluminous, highly evolved carbonatite: A microanalytical study of carbonate minerals from the Bayan Obo Deposit, China. *Econ. Geol.* **119**, 373–393 (2024).
14. W. L. Song, C. Xu, M. P. Smith, A. R. Chakhmouradian, M. Brenna, J. Kynicky, W. Chen, Y. H. Yang, M. Deng, H. Y. Tang, Genesis of the world's largest rare earth element deposit, Bayan Obo, China: Protracted mineralization evolution over similar to 1 b.y. *Geology* **46**, 323–326 (2018).
15. Z. L. Zhou, G. Y. Li, T. Y. Song, Y. G. Liu, Geological features and genesis of dolomitic carbonatite in Bayan Obo, Inner Mongolia (in Chinese). *Geol. Rev.* **26**, 35–41 (1980).
16. M. P. Smith, L. S. Campbell, J. Kynicky, A review of the genesis of the world class Bayan Obo Fe-REE-Nb deposits, Inner Mongolia, China: Multistage processes and outstanding questions. *Ore Geol. Rev.* **64**, 459–476 (2015).
17. K. Y. Wang, H. R. Fan, K. F. Yang, F. F. Hu, C. M. Wu, F. Y. Hu, Calcite-dolomite geothermometry of Bayan Obo carbonatites. *Acta Petrol. Sin.* **26**, 1141–1149 (2010).

18. K. Y. Wang, H. R. Fan, K. F. Yang, F. F. Hu, Y. G. Ma, Bayan Obo carbonatites: Texture evidence from polyphase intrusive and extrusive carbonatites. *Acta Geol. Sin.* **84**, 1365–1376 (2010).
19. X. K. Zhu, J. Sun, C. X. Pan, Sm-Nd isotopic constraints on rare-earth mineralization in the Bayan Obo ore deposit, Inner Mongolia, China. *Ore Geol. Rev.* **64**, 543–553 (2015).
20. X. C. Li, K. F. Yang, C. Spandler, H. R. Fan, M. F. Zhou, J. L. Hao, Y. H. Yang, The effect of fluid-aided modification on the Sm-Nd and Th-Pb geochronology of monazite and bastnasite: Implication for resolving complex isotopic age data in REE ore systems. *Geochim. Cosmochim. Acta* **300**, 1–24 (2021).
21. Y. H. Yang, F. Y. Wu, Q. L. Li, Y. Rojas-Agramonte, J. H. Yang, Y. Li, Q. Ma, L. W. Xie, C. Huang, H. R. Fan, Z. F. Zhao, C. Xu, In Situ U-Th-Pb Dating and Sr-Nd Isotope Analysis of Bastnäsite by LA-(MC)-ICP-MS. *Geostand. Geoanal. Res.* **43**, 543–565 (2019).
22. Z. C. Liu, F. Y. Wu, Y. H. Yang, J. H. Yang, S. A. Wilde, Neodymium isotopic compositions of the standard monazites used in U Th Pb geochronology. *Chem. Geol.* **334**, 221–239 (2012).
23. X. C. Li, Y. X. Zhan, H. R. Fan, K. F. Yang, The REE mineralization and remobilization history of the giant Bayan Obo deposit, Inner Mongolia, China: Constraint from in-situ Sm-Nd isotopes of REE minerals (In Chinese with English Abstract). *Acta Petrol. Sin.* **38**, 2920–2932 (2022).
24. J. S. Stacey, J. D. Kramers, Approximation of terrestrial lead isotope evolution by a two-stage model. *Earth Planet. Sci. Lett.* **26**, 207–221 (1975).
25. B. Schoene, "U–Th–Pb Geochronology" in *Treatise on Geochemistry*, H. D. Holland, K. K. Turekian, Eds. (Elsevier, ed. 2, 2014), pp. 341–378.
26. Y. Yu, Y. Li, Y. Liu, X. X. Ling, L. G. Wu, L. Yang, L. Yang, B. Yang, Y. G. Zhao, X. H. Li, Three-stage niobium mineralization at Bayan Obo, China. *Natl. Sci. Rev.* **11**, nwae063 (2024).
27. H. R. Fan, F. K. Chen, K. Y. Wang, Y. H. Xie, S. Wilde, M. Stair, Zircon U-Pb age of a carbonatite dyke from Bayan Obo REE-Fe-Nb deposit, Inner Mongolia and its geological, significance. *Acta Petrol. Sin.* **18**, 363–368 (2002).
28. H. R. Fan, F. F. Hu, F. K. Chen, K. F. Yang, K. Y. Wang, Intrusive age of No. 1 carbonatite dyke from Bayan Obo REE-Nb-Fe deposit, Inner Mongolia: with answers to comment of Dr. Le Bas. *Acta Petrol. Sin.* **22**, 519–520 (2006).
29. M. J. Lebas, Re-interpretation of zircon date in a carbonatite dyke at the Bayan Obo giant REE-Fe-Nb deposit, China. *Acta Petrol. Sin.* **22**, 517–518 (2006).
30. L. S. Campbell, W. Compston, K. N. Sircombe, C. C. Wilkinson, Zircon from the East Orebody of the Bayan Obo Fe-Nb-REE deposit, China, and SHRIMP ages for carbonatite-related magmatism and REE mineralization events. *Contrib. Mineral. Petrol.* **168**, 23 (2014).
31. S. H. Zhang, Y. Zhao, Y. S. Liu, A precise zircon Th-Pb age of carbonatite sills from the world's largest Bayan Obo deposit: Implications for timing and genesis of REE-Nb mineralization. *Precambrian Res.* **291**, 202–219 (2017).
32. X. C. Li, H. R. Fan, X. Zeng, K. F. Yang, Z. F. Yang, Q. W. Wang, H. T. Li, Identification of ~1.3 Ga hydrothermal zircon from the giant Bayan Obo REE deposit (China): Implication for dating geologically-complicated REE ore system. *Ore Geol. Rev.* **138**, 104405 (2021).
33. Y. S. Huang, X. C. Li, X. W. Xu, Q. L. Li, Q. Guo, Y. Liu, G. Q. Tang, X. H. Li, H. R. Fan, New discovery of the Early Paleozoic carbonatite in Bayan Obo (China): Insights into the giant REE accumulation. *Ore Geol. Rev.* **170**, 106156 (2024).
34. G. M. Yaxley, M. Anenburg, S. Tappe, S. Decree, T. Guzmics, Carbonatites: Classification, Sources, Evolution, and Emplacement. *Annu. Rev. Earth Planet. Sci.* **50**, 261–293 (2022).
35. H. D. She, H. R. Fan, M. Santosh, X. C. Li, K. F. Yang, Q. W. Wang, W. Wei, Y. J. Liu, S. Liu, S. L. Liu, Paleozoic remelting of carbonatite in Bayan Obo (China): Further insights into the formation of a giant REE deposit. *Gondw. Res.* **119**, 172–185 (2023).
36. L. Yang, Y. Li, Y. Liu, X. X. Ling, L. G. Wu, Y. Yu, L. Yang, W. X. Meng, G. Y. Yan, X. H. Li, Lead-lead dating reveals permian remobilization of niobium mineralization at Bayan Obo. *Econ. Geol.* **119**, 1383–1391 (2024).
37. M. P. Smith, Metasomatic silicate chemistry at the Bayan Obo Fe-REE-Nb deposit, Inner Mongolia, China: Contrasting chemistry and evolution of fenitising and mineralising fluids. *Lithos* **93**, 126–148 (2007).
38. M. P. Smith, P. Henderson, Preliminary fluid inclusion constraints on fluid evolution in the Bayan Obo Fe-REE-Nb deposit, Inner Mongolia, China. *Econ. Geol.* **95**, 1371–1388 (2000).
39. H. R. Fan, Y. H. Xie, K. Y. Wang, K. J. Tao, REE daughter minerals trapped in fluid inclusions in the giant Bayan Obo REE-Nb-Fe deposit, Inner Mongolia, China. *Int. Geol. Rev.* **46**, 638–645 (2004).
40. A. E. Williams-Jones, A. A. Migdisov, I. M. Samson, Hydrothermal mobilisation of the rare earth elements—A tale of "Ceria" and "Yttria". *Elements* **8**, 355–360 (2012).
41. M. P. Smith, P. Henderson, L. S. Campbell, Fractionation of the REE during hydrothermal processes: Constraints from the Bayan Obo Fe-REE-Nb deposit, Inner Mongolia, China. *Geochim. Cosmochim. Acta* **64**, 3141–3160 (2000).
42. M. Anenburg, J. A. Mavrogenes, C. Frigo, F. Wall, Rare earth element mobility in and around carbonatites controlled by sodium, potassium, and silica. *Sci. Adv.* **6**, eabb6570 (2020).
43. X. Yuan, R. Zhong, X. Xiong, J. Gao, Y. Ma, Transition from carbonatitic magmas to hydrothermal brines: Continuous dilution or fluid exsolution? *Sci. Adv.* **9**, eadh0458 (2023).
44. W. L. Song, C. Xu, M. P. Smith, J. Kynicky, J. Yang, T. Liu, D. Jing, Origin of heavy rare earth element enrichment in carbonatites. *Geochim. Cosmochim. Acta* **362**, 115–126 (2023).
45. X. Z. Hou, Z. F. Yang, Z. J. Wang, The occurrence characteristics and recovery potential of middle-heavy rare earth elements in the Bayan Obo deposit, Northern China. *Ore Geol. Rev.* **126**, 103737 (2020).
46. A. Banerjee, R. Chakrabarti, A. Simonetti, Temporal evolution of $\delta^{44/40}$Ca and ^{87}Sr/^{86}Sr of carbonatites: Implications for crustal recycling through time. *Geochim. Cosmochim. Acta* **307**, 168–191 (2021).
47. C. L. Li, X. G. Li, G. Y. Xu, Technology development and industrialization of resources comprehensive utilization of intergrowth and associated ore in Baiyun Obo. *Chin. Rare Earths* **36**, 151–158 (2015).
48. Y. T. Xu, R. C. Wang, M. F. Zhou, F. Y. Wu, Cassiterite and Sn mineralization in the giant Bayan Obo Fe-Nb-REE deposit, North China. *Am. Mineral.* **110**, 101–113 (2024).
49. A. R. Woolley, D. K. Bailey, The crucial role of lithospheric structure in the generation and release of carbonatites: geological evidence. *Mineral. Mag.* **76**, 259–270 (2012).
50. Y. Ying, W. Chen, J. Lu, S. Y. Jiang, Y. Yang, In situ U–Th–Pb ages of the Miaoya carbonatite complex in the South Qinling orogenic belt, central China. *Lithos* **290–291**, 159–171 (2017).
51. Institute of Geochemistry, Chinese Academy of Sciences, *Chinese, Geochemistry of Bayan Obo Ore Deposit* (Press of Science, 1988).
52. L. J. Drew, Q. R. Meng, W. J. Sun, The Bayan Obo iron–rare-earth–niobium deposits, Inner-Mongolia, China. *Lithos* **26**, 43–65 (1990).
53. H. R. Fan, K. F. Yang, F. F. Hu, S. Liu, K. Y. Wang, The giant Bayan Obo REE-Nb-Fe deposit, China: Controversy and ore genesis. *Geosci. Front.* **7**, 335–344 (2016).
54. Y. Y. Li. *Chinese, Geology and Exploration of the Bayan Obo Fe Deposit* (Geology Press, 1959).
55. X. H. Li, Y. Liu, Q. L. Li, C. H. Guo, K. R. Chamberlain, Precise determination of Phanerozoic zircon Pb/Pb age by multicollector SIMS without external standardization. *Geochem. Geophys. Geosyst.* **10**, Q04010 (2009).
56. M. Wiedenbeck, P. Allé, F. Corfu, W. L. Griffin, M. Meier, F. Oberli, A. V. Quadt, J. C. Roddik, W. Spiegel, Three natural zircons standards for U-Th-Pb, Lu-Hf, trace element and REE analyses. *Geostandard. Newslett.* **19**, 1–23 (1995).
57. L. P. Black, S. L. Kamo, I. S. Williams, R. Mundil, D. W. Davis, R. J. Korsch, C. Foudoulis, The application of SHRIMP to Phanerozoic geochronology; a critical appraisal of four zircon standards. *Chem. Geol.* **200**, 171–188 (2003).
58. P. Vermeesch, IsoplotR: A free and open toolbox for geochronology. *Geosci. Front.* **9**, 1479–1493 (2018).
59. Y. Li, D. Selby, X. H. Li, C. J. Ottley, Multisourced metals enriched by magmatic-hydrothermal fluids in stratabound deposits of the Middle–Lower Yangtze River metallogenic belt. *Geology* **46**, 391–394 (2018).
60. D. Selby, K. D. Kelley, M. W. Hitzman, J. Zieg, Re-Os sulfide (bornite, chalcopyrite, and pyrite) systematics of the carbonate-hosted copper deposits at Ruby Creek, Southern Brooks Range, Alaska. *Econ. Geol.* **104**, 437–444 (2009).
61. Y. Li, P. Vermeesch, Short communication: Inverse isochron regression for Re–Os, K–Ca and other chronometers. *Geochronology* **3**, 415–420 (2021).
62. Y. S. Liu, Z. C. Hu, K. Q. Zong, C. G. Gao, S. Gao, J. Xu, H. H. Chen, Reappraisement and refinement of zircon U-Pb isotope and trace element analyses by LA-ICP-MS. *Chin. Sci. Bull.* **55**, 1535–1546 (2010).
63. P. B. Tomascak, E. J. Krogstad, R. J. Walker, U-Pb Monazite Geochronology of Granitic Rocks from Maine: Implications for Late Paleozoic Tectonics in the Northern Appalachians. *J. Geol.* **104**, 185–195 (1996).
64. L. Chen, Y. S. Liu, Z. C. Hu, S. Gao, K. Q. Zong, H. H. Chen, Accurate determinations of fifty-four major and trace elements in carbonate by LA-ICP-MS using normalization strategy of bulk components as 100%. *Chem. Geol.* **284**, 283–295 (2011).
65. X. X. Ling, Q. L. Li, Y. Liu, Y. H. Yang, Y. Liu, G. Q. Tang, X. H. Li, In situ SIMS Th–Pb dating of bastnaesite: constraint on the mineralization time of the Himalayan Mianning–Dechang rare earth element deposits. *J. Anal. At. Spectrom* **31**, 1680–1687 (2016).
66. L. G. Wu, X. H. Li, X. X. Ling, Y. H. Yang, C. F. Li, Y. L. Li, Q. Mao, Q. L. Li, B. Putlitz, Further Characterization of the RW-1 Monazite: A new working reference material for oxygen and neodymium isotopic microanalysis. *Minerals* **9**, 583 (2019).
67. A. R. Woolley, B. A. Kjarsgaard, Paragenetic types of carbonatite as indicated by the diversity and relative abundances of associated silicate rocks: Evidence from a global database. *Can. Mineral.* **46**, 741–752 (2008).
68. S. L. Liu, L. Ma, X. Zou, L. Fang, B. Qin, A. E. Melnik, U. Kirscher, K. F. Yang, H.-R. Fan, R. N. Mitchell, Trends and rhythms in carbonatites and kimberlites reflect thermo-tectonic evolution of Earth. *Geology* **51**, 101–105 (2022).
69. E. R. Humphreys-Williams, S. Zahirovic, Carbonatites and Global Tectonics. *Elements* **17**, 339–344 (2021).

70. V. I. Berger, D. A. Singer, G. J. Orris, *Carbonatites of the World, Explored Deposits of Nb and REE-database and Grade and Tonnage Models*. (U. S. Geological. Survey, 2009); https://pubs.usgs.gov/of/2009/1139/.

Acknowledgments: We thank K.-Y. Wang and F.-Y. Hu for leading the fieldtrip in 2019 and sharing their 60-year expertise on Bayan Obo. We thank J.-Y. Liu, Y.-G. Zhao, F. Cui, G.-Y. Yan, M.-Z. Hao, J.-J. Yang, and B. Yang from Baotou Iron and Steel Group for supporting multiple visits in the mining area. We thank D.-M. Guan for logistical support and driving during our field trips. Z.-C. Hu and T. Luo are thanked for conducting bastnäsite and monazite ^{232}Th-^{208}Pb dating at China University of Geosciences, Wuhan. C. Ottley and G. Nowell are thanked for laboratory support at Durham University. D.-F. Li and Q.-F. Liu helped with CL imaging at Sun Yat-sen University. We thank R.-W. Ge and Z.-L. Shi for drafting Fig. 6. Q. Hu and L.-H. Yao are thanked for their assistance in collecting the data for Fig. 1 and fig. S11. We thank the reviewers for their constructive comments and criticisms, which have clarified our thoughts and improved the presentation. **Funding:** This work was supported by the National Natural Science Foundation of China grants 42325303 (to Y.L.) and 92262303 (to X.-H.L.). **Author contributions:** Conceptualization: Y.L. and X.L. Methodology: Y.L., X.-H.L., and D.S. Investigation: Y.L., L.-G.W., Y.Y., and L.Y. Visualization: Y.L. Supervision: Y.L., X.-H.L. Funding: Y.L. and X.-H.L. Writing—original draft: Y.L. Writing—review and editing: Y.L. with inputs from all authors. **Competing interests:** The authors declare that they have no competing interests. **Data and materials availability:** All data needed to evaluate the conclusions in the paper are present in the paper and/or the Supplementary Materials.

Submitted 4 September 2024
Accepted 19 March 2025
Published 23 April 2025
10.1126/sciadv.ads9481